Preparation and characterization of organo-functionalized silicas for bilirubin removal

UNIVERSITÀ DEGLI STUDI DI TORINO

Preparation and characterization of organo-functionalized silicas for bilirubin removal

Alexander S. Timin [a,*], Evgeniy V. Rumyantsev [a], Alexey V. Solomonov [a], Irek I. Musabirov[b,1], Semen N. Sergeev[b,1], Sergey P. Ivanov[c], Gloria Berlier[d], Elena Balantseva[d]

[a] Inorganic Chemistry Department, Ivanovo State University of Chemistry and Technology (ISUCT), 7, Sheremetevsky Prosp., 153000 Ivanovo, Russian Federation

[b] Institute for Metals Superplasticity Problems of Russian Academy of Sciences, St. Khalturina Str. 39, 450001 Ufa, Russian Federation

[c] Institute of Organic Chemistry, Ufa Science Centre of the Russian Academy of Sciences, 71 Prosp. Oktyabrya, 450054 Ufa, Russian Federation

[d] Università di Torino, Dipartimento di Chimica and NIS (Nanostructed Interfaces and Surfaces) Centre, via P. Giuria 7, 10125 Torino, Italy

Abstract

Hybrid-silica materials containing octyl, phenyl and urea-propyl functional groups were reported. These functionalized silicas were prepared by a via one-pot synthesis method through co-condensation of tetraethyl ortosilicate with organosilanes co-precursors. The obtained materials were analyzed by a number of techniques including scanning electron microscopy, Fourier transform infrared spectroscopy,

X-ray diffraction pattern and nitrogen sorption measurement. The main elements: morphology and surface properties of the final products that are basically dependent on the type and the quantity of functional-containing groups were fully discussed. The adsorption properties of the modified silicas were investigated against bilirubin in aqueous solution at pH 7.4, the effect of time was studied as well. The modified silicas showed a greatly increasing of adsorption capacity for bilirubin compared to pure amorphous silica. The results indicate that the type of functional-containing groups and surface properties affect the adsorption behavior. These materials show a potential application as effective adsorbents for bilirubin removal.

*Corresponding author. Tel.: +7 910 669 36 43.

E-mail addresses: a timin@mail.ru (A.S. Timin), evr@isuct.ru (E.V. Rumyantsev).

Tel.: +7 347 282 37 51; fax: +7 347 282 37 59.1.

Introduction

Silica gel is an amorphous inorganic polymer composed of internal siloxane groups (Si–O–Si) with silanol groups (Si–OH) distributed on the surface. Nowadays, silica gel is widely used in many chemical processes to provide new technical application due to its valuable physical and structural characteristics such as a high chemical and thermal stability, a large surface area and a pore size, chemical inertness, and it is a great potential for fabricating nanostructures [1–4].

Moreover, modified silica gels have increased their potential application in many scientific and technological branches such as a high performance liquid chromatography (HPLC)

bonded phases for specific separations, supports for catalysts in specific organic reactions, supports for microorganism and pesticides [5], and the extractions of metallic cations from aqueous and non aqueous solvents by forming immobilized metallic complexes [6]. Modification of silica surface can be achieved via several methods: (1) functionalization with organic functional groups [7]; (2) via a physical adsorption of active species leading to a variety of useful supported reagents [8]; (3) modification via incorporation of natural or synthetic polymers [9–11]. Functionalization of mesoporous silicas with silane-coupling agents via two-steps methods has attracted considerable attention [12,13]. This is mostly due to its a large surface area and pore size in comparison to nonporous silica [14]. Several mesoporous silicas have been functionalized with different ligands and intensively investigated over the last decade [14–17]. Moreover, at present time the preparation of organo-functionalized mesoporous silicas using one-pot synthesis method have been received much attention [18,19]. According to the grafting two-step method of synthesis, the population of the organic groups is limited to the original number of surface silanols on the mesoporous silica, and thus, a low surface coverageis obtained [20]. The most promising method is based on one-pot synthesis [22]. In recently published article [21] the one-pot grafting method of polystyrene on polydopamine coated silica particles was investigated. The obtained results showed that one-pot grafting approach exhibited higher grafting density when compared to two-steps grafting strategy. What is more, the nature of functional groups grafted on silica surface plays an important role in the surface properties of modified materials such as a hydrophobicity and a chemical reactivity [2,22] what makes its great potential to use these materials in drug delivery systems or a treatment of different toxicological diseases.

One of the well-known endogenous toxins is bilirubin [23].

Bilirubin is a pathogenic substance and one of the products of hemoglobin's metabolism. Normally, bilirubin is transported tothe liver as a complex with albumin where it is conjugated with glucuronic acid and excreted into bile [24,25]. However, when the bilirubin concentration in plasma is higher than the normal level (>15 mg/dL), it is usually caused by pathogenic liver disease.

Moreover, the extra free bilirubin binds and deposits onto carious tissues, including the brain tissues [26]. Many techniques have been employed for the removal of a high concentration of bilirubin from plasma in order to prevent the liver disease and brain damage such as plasma apheresis, hemodyalysis, photocatalytic or affinity membrance chromatography [26]. However, hemoperfusion treatment is one of the most effective techniques at the moment [27,28]. This technique is based on the circulation of blood through a special unit containing an adsorbent for bilirubin removal. So, bilirubin interaction with various compounds which then might be used for surface modification of the adsorbent is interesting subject of many publications [29–32]. Due tothe fact that bilirubin has several hydrophobic and hydrophilicreaction sites in its structure and also contains carboxyl and iminegroups, the interactions of matrices with tetrapyrrole may be carried out by various ways [23,29]. Conformational state of bilirubinalso plays a significant role during the interaction processes. The“ridge-tile” conformation of the pigment is one of the most stable conformations in majority of solutions and solids (Fig. 1) when binding processes are investigated. It was reported by McDonagh group the additional interactions between bilirubin molecule and protein occur via hydrogen-bonding of the carbonyl oxygen in the protein and two nitrogen atoms of bilirubin [23]. It was shownwhen considering the bilirubin and -cyclodextrin binding, that the hydrophobic interactions can play a critical role for inclusionability for bilirubin [33]. It was shown that extra free bilirubin can be attached to cyclodextrine (CD) family via electrostatic forces [34]. Another work [35] describes a complex formation of poly(zincprotoporphyrin-methacrylic acid-ethyl glycol dimethylacrylate) matrix (ZnPP) with bilirubin. It is established that the four pyrrole-rings of ZnPP could form stacking interaction with the four-pyrrole rings of bilirubin. The zinc in the ZnPP structure could further coordinate with bilirubin to form much rigid recognition sites in the matrix. To sum up, we can conclude that the different mechanisms of bilirubin interaction with various substances can be successfully applied to develop a new approaches of bilirubin utilization from the human organism [36]. Up to now, several adsorbents with different physical and chemical characteristics were used for bilirubin removal. In recent article [37], bilirubin adsorption capacities on single-wall carbon nanohorns (SWNHs) were investigated. Authors showed that bilirubin is selectively adsorbed to the SWNHs, especially to the SWNHs with high oxidation levels against albumin simultaneously mixed insolution. In another paper [38], the analysis of the bilirubin adsorption confirmed the possibility of electrostatic interactions between bilirubin molecules and guanidine polymers incorporated inside silica matrix.

Although a lot of publications concerning the preparation of surface-modified silica particles have been written but the effect of functional groups on the surface properties, morphological structure and, therefore, their influence on the bilirubin adsorption arenot clearly understood. Here, a

comparative study of the influence of organosilane co-precursors on the morphological structur eof the final products and bilirubin adsorption from aqueous solution at pH 7.4 has been performed. The adsorbents for bilirubin removal were prepared using tetraethyl ortosilicate and organosilane co-precursors as starting materials for surface modification.

Octyltriethoxysilane and phenyltriethoxysilane were chosen as the agents for modification due to the presence of octyl and phenyl functional groups exhibiting hydrophobic properties. The 1-[3-(trimethoxysilyl)-propyl]urea was chosen because of the presence of amine and carboxyl functional groups. For all hybrid materials ratios of tetraethyl ortosilicate and organosilane co-precursors were employed, to explore the effect of this parameter on their properties.

2. Experimental

2.1. Materials and methods

Octyltriethoxysilane CH3(CH2)7Si(OC2H5)3 (OTES ≥97.5%),phenyltriethoxysilane C6H5Si(OC2H5)3(PhTES≥98%),1-[3-(trimethoxysilyl)-propyl]urea (CH3O)Si(CH2)3NHCONH2(TMSPU ≥ 97%) were purchased from Aldrich (USA). Tetraethylortosilicate Si(OC2H5)4(TEOS ≥ 98%) was supplied by commercial chemical Company "Ecos-1" (Russian Federation). Bilirubin(Mw= 584.7 g/mol) was purchased from Sigma–Aldrich (USA). Aqueous solutions at pH 7.4 were prepared by dissolving bilirubinin alkaline solution lowering the pH by addition of phosphate buffer and filtering the prepared solution to remove any solid bilirubin. Absolute ethanol and ammonia solution (25 wt% ammonia) were obtained from "Ecos-1" (Russian Federation). The chemicals were analytical grade and were used without further purification. Deionized water was used in these experiments.

2.2. Synthesis of non-functionalized silica.

The synthesis route of non-functionalized silica is rather typical and it was already described in [39]. In a typical synthesis, it was used TEOS and H2O in relative molar ratios of 1:4. For this rea-son, 8.13 g of TEOS was added in 22.66 g of water–ethanol solution containing 2.66 g of water and 20 g of ethanol. Then this obtained mixture was stirred for 2 h. The 0.005 ml ammonia solution (pH8) was added every 20 min during 2 h. After that the mixture was transferred into a Petri dish and was aged for 3 days until the formation of silica particles The solid product was washed with de-ionized water and ethanol, and then dried for 2 days at 95 ◦C under vacuum.

2.3. Synthesis of octyl functionalized silicas.

Octyl functionalized silica (OctSiNP-1) was prepared following an approach schematized in Fig. 2. More in detail, 6.48 g of TEOS and 1.82 g of OTES were added into water–ethanol solution containing 2.66 g of de-ionized water and 20 g of ethanol. The ammonia solution was used as a base catalyst. The molar composition of the initial mixture was 4:1 = TEOS/OTES. After stirring for 2 h at room temperature, the obtained homogeneous mixture was transferred into a Petri dish and was aged for 3 days until the formation of the ultra-disperse silica particles. The solid product was washed with de-ionized water and ethanol, and then dried for 2 days at 95◦Cunder vacuum. The synthesis of other octyl modified samples was the same to the one above described. The weights of TEOS, OTES and the molar ratio of TEOS/OTES are shown in Table 1.

2.4. Synthesis of phenyl functionalized silicas.

The method for functionalization of amorphous silica gel byphenyl groups is familiar to above described and is illustrated for all functional groups in Fig. 2. The phenyltriethoxysilane was used for surface modification. In order to prepare a sample with the lowest phenyl-containing groups (PhSiNP-1) the mixture containing6.48 g of TEOS and 1.88 g of PhTES was added to solution consisting of 20 g of ethanol and 2.66 g of de-ionized water and stirred for 2 h at room temperature. Also the ammonia solution (pH 8) was added as a base catalyst during 2 h. Then the obtained mixture was transferred into a Petri dish and was aged for 3 days until the formation the ultra-disperse silica particles. Then the solid phase was separated and washed with de-ionized water and ethanol. After that, it was dried under vacuum at 95◦C for 2 days. The same process was repeated for other samples modified with phenyl groups.

The weights of TEOS, PhTES and the molar ratio of TEOS/PhTES are shown in Table 1.

2.5. Synthesis of urea-propyl functionalized silicas

For preparation of urea-propyl functionalized silicas (Fig. 2), the1-[3-(trimethoxysilyl)-propyl]urea was used. Typically for synthesis of USiNP-1, 6.48 g of TEOS and 1.74 g of TMSPU were mixed and added to the water–ethanol solution containing 20 g of ethanol and2.66 g of de-ionized water. The reaction mixture was stirred for further 2 h at room temperature by adding the ammonia solution. After that the obtained mixture was aged during 3 days. The final precipitate was collected by filtration, washed with water–ethanol solution and dried under vacuum at 95◦C for 2 days. The weights of TEOS, TMSPU and the molar ratio of TEOS/TMSPU for all prepared samples are shown in Table 1.

2.6. Characterization of the obtained materials

X-ray diffraction analysis of the powder samples was performed using a Bruker X-ray diffractometer D8 Advance. X-ray source was Ni-filtered MoK$_{\text{ˌ}}$ radiation. The X-ray source operating voltage was40 kV and the scan rate was 2/min. The nitrogen adsorption and desorption isotherms were measured at 77 K on a Micromeritics ASAP 2020 m instrument (Micromeritics Instrument Corp., Nor-cross, GA). The Brunauer–Emmett–Teller (BET) specific surface area was calculated using adsorption data. The pore size distribution curves were calculated from the analysis of the adsorption branch of the isotherm using the Barrett–Joyner–Halenda algorithm. Error in determining of BET surface area and pore volume are estimated to be within 5%. The Fourier transformed infrared spectroscopy (FTIR) spectroscopy was performed on a NicoletTM4700 FTIR spectrometer ("Nicolet", USA). The transmittance measurements were carried out according to the KBr technique. The spectra were performed in the 4000–400 cm^{-1} range. The scanning electron microscope (SEM, 20 kV) images were taken on high resolution scanning electron microscope Tescan Mira-3LMH. Before examining, all the samples were dissolved in ethanol. The obtained emulsion was coated onto the polished surface of aluminum table. The obtained samples were kept for a day under vacuum (10 −2Pa). Electron microscopic studies were carried out at accelerating voltage of 20 kV. The analysis of the particle size distribution for all prepared samples is based on ASTM E112-12 (Standard Test Methods for Determining Average Grain Size). All prepared samples (about 1000 particles of every sample) were analyzed in two dimensions. The obtained quantitative data were statistically processedand then the histograms of particle size distribution were built.

2.7. Adsorption of bilirubin on the functionalized and amorphous silicas

All bilirubin samples with various mass (stored in dark at 15◦C) were dissolved in a small amount (0.2 ml) of alkaline solution (NaOH, C = 0.2 mol/l) with pH 13. After complete dissolution and intensive mixing during 5 min, bilirubin solutions in NaOH were diluted by addition of phosphate buffer (NaH2PO4/Na2HPO4, pH7.4) and filtered the prepared solution to remove solid bilirubin if any remained. The solutions obtained (4 ml) were also stored in dark at 15◦C and fully employed within the following 2 h. The prepared water solutions with different concentration of bilirubin were used for adsorption experiments. In every experiment, 125 mg of adsorbent and 10 ml of bilirubin solution were mixed and stirred at 25◦C. After the adsorption equilibrium has been attained, the solution was separated by centrifugation. The concentration of bilirubin in water solution before and after adsorption was determined by UV–visible spectrophotometer SF-104 ("Aquilon", Russian

Federation) at 440 nm. The pH values were measured by a pH-meter U-500 (“Aquilon”, Russian Federation). Confidence intervals of 95% were calculated for all samples, to determine the margin of error. The amount of bilirubin adsorbed onto silica surface (mg/g) was calculated by the following equation:

$$q = \frac{V(C_0 - C)}{m} \quad (1)$$

where C_0 and C are the initial and the residual bilirubin concentration in solution (mg/ml), V is the volume of bilirubin solution (in ml), m is the mass of the adsorbent (in g), respectively.

3. Results and discussion

3.1. FTIR spectra

The FTIR spectra of non-functionalized and functionalized silicas revealed several bands which are assigned to the various structural units and surface groups of the silica matrix. Fig. 3demonstrates the FTIR spectra of SiNP, OctSiNP-3, PhSiNP-3 andUSiNP-3, respectively. There are minor differences for other samples with a different quantity of functional-containing groups so we presented only FTIR spectra of samples with high-test quantity of grafting functional groups. The analysis of the FTIR spectra of the synthesized silicas is presented below. All major vibrations frequencies and their corresponding structural units are shown in Table 2 for better comprehension. Analysis of FTIR spectra of pure amorphous silica and octyl modified silicas revealed the broad band in the range 3558–3346 cm^{-1} corresponding to the O–H stretching bands of hydrogen-bonded water molecules and SiO–H stretching vibrations [40]. The corresponding Si–OH bending mode is found at 948 cm^{-1}. The “bulk” vibrational modes corresponding to SiO4 groups are observed at 1087–1095 cm^{-1}, 800 cm^{-1} (antisymmetric and symmetric Si–O–Si vibrations, respectively), with the bending vibrations at 458–457 cm^{-1} [41]. The FTIR spectra of octyl modified silicas (Fig. 3) show the described modes of amorphous silica with clear bands between2989 and 2848 cm^{-1} (intensive asymmetric and symmetric C–H stretching vibrations, 1640, 1615 and 1384 cm^{-1}. The band at1384 cm^{-1} can be assigned to the antisymmetric bending mode of the CH3 unit [42]. The phenyl functionalized silicas (PhSiNP-3). These show in addition weak peaks around 2989–2919 cm^{-1} (C–H antisymmetric and symmetric vibrations) probably due to small amounts of contaminants. The presence of the phenyl groups is

testified by bands at 1432 and1384 cm^{-1}, which can be assigned to the aromatic ring vibrations. The sharp weak peaks at 1432 cm^{-1} corresponds to the combination of two vibrations: phenyl C=C stretching vibrations and in-plane C–H deformation [42]. It is also observed that the intense band corresponding to the asymmetric Si–O stretching vibrations is separated into two peaks: one small weak at 1135 cm^{-1} and another very intensive at 1078 cm^{-1}. This could be related to a distortion induced by the insertion of the phenyl groups in the silica matrix. The narrow peaks at 700 cm^{-1} are assigned to the phenyl out-of-plane ring deformation vibration [42,43]. The FTIR spectra of urea-propyl modified silicas revealed the same bands which also typical for pure silica and other organo-functionalized silicas: the Si–O–Si stretching bands at 1066 cm^{-1} belongs to the USiNP-1; the broad peak between 3544 and 3353 cm^{-1} corresponds to the water adsorbed onto silica surface. The bands of C–H groups are very weak and located at about 2933 cm^{-1}. The difference between FTIR spectra of urea-propyl modified silicas and non-functionalized silica can be associated with the presence of intense peaks in the range of1672–1590 cm−1corresponding to the amide carbonyl stretching vibrations known as the (C=O) amide I [39,44] and the (N–H) amide II [39,44,45], respectively. Thus, we can conclude that silica surface were successfully modified using the combination of silicon precursors and co-precursors that were confirmed the existence of different chemical groups corresponding to the functional groups of silicon precursors and co-precursors.

3.2. X-ray diffraction analysis of organo-functionalized silicas

XRD patterns of pure silica and samples with the highest concentration of functional-containing groups are shown in Fig. 4. XRD patterns of the organo-functionalized silicas and pure silica gel produce broad scattering peaks around at 20–25 ◦ which assigned to the typical structure of amorphous silica. As demonstrated Fig. 4, four peaks with different intensity were observed for all samples. These four peaks correspond to the interatomic distances in silica matrix. A small difference in the intensity of these peaks for SiNP, OctSiNP-3, UPSiNP-3 and PhSiNP-3 indicates minor changes in geometrical structure of synthesized samples related to the influence of func-tional groups grafted onto silica surface. According to the literature [46–48] the position of the peak s4 (s4≈ 3.18–3.31 $Å^{-1}$) corresponds to the distance range ≈ 2 π/s ≈ 1.97–1.89 Å which is typical for Si–O interatomic

distance. The peaks (s3) up to s ≈ 1.65 $Å^{-1}$ or r ≈ 3.80 Å are determined by the Si–Si distance [48]. However, the peak (s3) is very broad and weak in case of pure silica. This suggests an effect of the different silica condensation rates when using different organosilanes during sol–gel synthesis. The weak peak (s1) at 0.46 $Å^{-1}$ can be clearly indicated only for PhSiNP-3. This might be due to the formation of an ordered arrangement of pores in silica matrix (see below for textural properties discussion).

3.3. Scanning electron microscopy

To investigate the influence of grafted functional groups on the morphology and particle size of modified silicas, all prepared samples were examined by scanning electron microscopy (Figs. 5–7). The data of non-functionalized silica are not placed here because there were shown and discussed in our previous work [49]. The silica particles are of spherical shape and in size range from 200 to 400 nm. The particles are well define and do not form agglomerates. Fig. 5 represents the typical SEM images of urea-propylfunctionalized silicas. As for urea-propyl functionalized silicas, spherical particles are not uniform in size as can be clearly observed from the SEM images and corresponding particle size distribution. The particle size distribution of the USiNP-1 extended from 0.35 μm to 5.25 μm, with average size of 2.41 ± 0.30 μm. The most abundant measured size are 1.10 μm, 2.50 μm and 3.20 μm (26%,30% and 25%, respectively). By comparing the three urea-propyl functionalized silicas an increase in average size and related standard deviation is observed. This indicate that an increase of thecontent of TMSPU during sol–gel synthesis favors the formation ofbig spherical clusters of silica particles. The SEM images of phenyl functionalized silicas are shown in Fig. 6 demonstrating significant difference in morphology and particle size distribution compared to urea-propyl functionalized silicas. The SEM images of phenyl-functionalized silicas show the presence of different non-uniform particles and particle agglomerates. We can conclude that the application of phenyltriethoxysilane in sol–gel synthesis leads to the formation of plate like structure. This might be explained by the high rate of hydrolysis and polycondensation of phenyltriethoxysilane. These properties thus favor the formation of big non-uniform cluster agglomerates. The obtained histograms of particles size distribution show the influence of phenyl quantity on average particle sizes. The particle size distribution of PhSiNP-1 ranges from 0.5 to 33 μm with them most abundant populations between 1.98 and 4.01 μm. The average particle size is about 2.19 μm. However, big particle agglomerates of 10, 12 and even 20 μm can also be observed PhSiNP-2 is characterized by particle sizes between 2 and 17 μm, with more abundant ones in the range from 4 to 8 μm. A further increase

of average particle size is observed in the case of PhSiNP-3, indicating also in this case an effect of the phenyl-containing functional group concentration on the growth of silica agglomerates. The SEM images of octyl functionalized silicas revealed that they have spherical morphology. What is more, it can be seen that all samples (Fig. 7) exhibited nanostructure with uniform spherical nanoparticles uniform in size. The influence of octyl-containing groups on particle size distributions can be inferred from the corresponding histograms (Fig. 7). The particle size of OctSiNP-1ranges from 66 to 174 nm and the average particle size is about112 ± 21 nm. The main peak corresponding to the average particle size equals to 149 ± 36 nm in case of OctSiNP-2, while the sample with highest octyl-containing groups is characterized by the narrowest particle size distribution with a mean value of 167 ± 23 nm. As observed for the other samples also in this case particle size increases with an increase of the functional groups. So, the investigation of the SEM images of all samples modified with urea-propyl, phenyl and octyl groups indicates that the size and the shape of the final products were fully dependent on quantity and the type of the used organo-precursors in sol–gel synthesis. The structure of final products is tunable by varying the molar ratio of used silicon precursors and co-precursors in sol–gel synthesis.

3.4. Surface area characterization

The nitrogen isotherms with the corresponding pore-size distribution for samples with a minimum and maximum content of functional groups are presented in Fig. 8. As it can be seen from Fig. 8, according to the IUPAC classification [50] the samples SiNP and PhSiNP-3 exhibit type I (SiNP) and type IV (PhSiNP-3) adsorption/desorption profiles, respectively. The typical hysteresis loop (type H2) is observed in case of PhSiNP-3. The hysteresis loop is usually associated with the filling and emptying of the mesopores by capillary condensation. However, the other samples modifying with octyl and urea groups show type IIb isotherms with type H3hysteresis associated to inter-particles pores originating from packing of particles. The isotherm of pure silica (SiNP) exhibits a very gradual increase of adsorbed nitrogen, suggesting a broad distribution of pores, which are however characterized by small volume (Table 3). In this case no hysteresis loop is observed, showing an important effect of the functional groups on silica porosity. The BET surface area of all samples along with their total pore volume and average pore size calculated according to the BJH methods are listed in Table 3. The obtained results show that the surface properties of modified silicas are clearly different from pure silica. The pure silica is characterized by a low specific surface area (~40 m^2/g). Also the pore size distribution curve of pure silica shows very intensive peak at 2.6 nm and one weak peak between 5 and 7 nm. The increase in the surface area, pore size and pore volume is observed

after surface functionalization for all silicas modified with octyl, phenyl and urea-propyl fragments. The specific surface area, average pore size of OctSiNP-1are 91 m^2/g and 16 nm while the specific surface area and average pore size of OctSiNP-3 are 85 m^2/g and 19 nm, respectively. This a minor effect of octyl functional groups on surface properties is observed. However, we can observe serious changes in surface area in case of phenyl modified silicas. The surface area of PhSiNP-1 equals166 m2/g whereas the surface area of PhSiNP-3 is 330 m2/g. The latter sample (PhSiNP-3) also shows a narrow pore size distribution with the average pore size of 6.5 mn whereas PhSiNP-1 is characterized by the broad pore size distribution with average pore size of 17 mn. This suggests an important effect of the phenyl functional groups concentration on the surface properties and porosity. By comparing these data to the SEM images it is clear that the sample (PhSiNP-3) shows the highest specific surface area but also the largest particle size. This apparent disagreement could be explained by an important role of the small pores in determining the overall surface area. Furthermore, the formation big clusters of agglomerates consisting of non-spherical particles might have an impact. The particle shape is an important factor in determining physic mechanical properties of colloidal systems and could be responsible for the formation of relatively small pores (6.5 nm), responsible for the high surface area. Analysis of experimental data of urea-propyl modified silicas confirmed the fact that increasing the amount of urea-propyl groups onto silica surface leads to a reduction in the surface area. This also results in a decrease of pore size which is probably due to the occupation of the functionalized molecules on the surface.

3.5. Adsorption of bilirubin from aqueous solution.

3.5.1. Effect of time

The effect of time on the bilirubin adsorption was studied (Fig. 9).The results show that adsorption rate depends on the type of the sed adsorbent. It appears that the adsorption kinetics of pure amorphous silica was faster than that of the modified silicas with different functional groups. The time required to reach equilibrium conditions was about 60 min in case of pure amorphous silica whereas the adsorption time of OctSiNP-3 and PhSiNP-3 for reaching equilibrium conditions was ~ 90 min. This was even higher forUSiNP-3 (~120 min). It can be also seen that the adsorption capacity of the modified adsorbents is higher than for pure silica. This fact might be due to specific Van der Waals, hydrogen bonding and electrostatic interactions, which could require a longer time to reach equilibrium conditions. Moreover, the differences in kinetics could be related to the different interparticle porosity of the samples. More details concerning the type of interactions between

bilirubin and functionalized silica surface will be discussed later. A wide range of adsorption rates have been reported in the literature.

From the analysis of literature [51] for patients diagnosed as having fulminant hepatitis it was reported that the effective treatment time for bilirubin removal ranges from 1 to 2 h. In this study it can be concluded that the time to reach equilibrium conditions seems to be quite suitable.3.5.2. Bilirubin adsorption isotherms. The relations between the equilibrium concentration of bilirubin and the equilibrium adsorption amount of bilirubin for all prepared samples are given in Fig. 10. The adsorption values of bilirubin increased as the bilirubin concentration increased, and finally reached a saturation level at high concentrations. It can be seen that up to a certain concentration, no more bilirubin can be adsorbed on the silica surface. Therefore, it can be estimated that the adsorption capacity of SiNP, OctSiNP-1,OctSiNP-2 and OctSiNP-3 for bilirubin are 0.32, 0.57, 0.64 and 0.73 mg/g, respectively. As for PhSiNP-1, PhSiNP-2 and PhSiNP-3, the adsorption capacity equals to 0.51, 0.71 and 0.95 mg/g, respectively. The adsorption capacity for USiNP-1,USiNP-2 and USiNP-3 is found to be 0.95,1.53 and 2.01 mg/g, respectively. The obtained results indicate that the adsorption capacity for bilirubin of functionalized adsorbents increased after surface modification.

It can be observed that the maximum amount of adsorbed bilirubin strongly depends on the type and quantity of used functional groups. It is clearly that the adsorption capacity of octyl and phenyl functionalized silicas is much higher than that of pure silica gel. Bilirubin is basically a hydrophobic molecule so its higher adsorption in case of silicas modified with octyl and phenyl groups can be probably related with the hydrophobic properties of octyl and phenyl groups. It was shown [52,53] that hydrophobic interactions play an important role in adsorption of dyes and drugs when the silica surface was modified by octyl and phenyl fragments. More-over, the pore volumes of OctSiNP-3 (0.48 cm^3/g) and PhSiNP-3(0.39 cm3/g) are sensibly larger than that of pure amorphous silica (0.015 m^3/g). This fact also plays an important role in increasing of adsorption capacity for bilirubin. The phenyl functionalized silicas exhibited a better value of adsorption capacity which can be associated with stronger hydrophobic attractions and higher surface area (SBET= 330 m^2/g for PhSiNP-3). The urea-propyl modified adsorbents seem to have the best adsorption capacity for bilirubinin aqueous solution with respect to the other prepared materials. In aqueous solutions, amine and carbonyl groups of urea fragment can be protonated and deprotonated. The lone pair of electrons on the nitrogen is delocalized into the carbonyl with formation of negative and positive charges, respectively [54]. In water at pH 7.4 two carboxyl groups in bilirubin molecule can dissociate with negative charge. Therefore, we can suggest that high adsorption capacity for bilirubin is observed due to existence of strong electro-static interactions between carboxyl groups of bilirubin and amine groups in urea fragment of modified silica. In addition, formation of hydrogen bonding between amide carbonyl

groups and carboxyl groups of bilirubin and non-specific Van der Waals interactions have influence on bilirubin adsorption. However, the surface area and porosity have also impact on increase of adsorption capacity with respect to bilirubin. Thus, the difference of bilirubin adsorption is mostly due to the properties of each adsorbent: the morphological structure,s pecific surface area, total pore volume and average pore size, functional groups grafted onto surface. Moreover, even if the amount of organic functionality was not determined in the pre-pared hybrid materials, an effect of the ratio between tetraethylortosilicate and organosilane co-precursors employed in the synthesis was observed in the adsorption efficiency. Therefore, we suppose that the type of surface functional groups has the strongest influence on bilirubin adsorption. The surface area of octyl- and urea-propyl modified silicas does not change remarkably in comparison with their adsorption capacities. Moreover, in spite of the highest surface area of phenyl modified silicas (S_{BET}= 330 m^2/g), the urea-propyl modified silica (SBET= 105 m2/g) is characterized by the highest adsorption. Also we suggest that spherical particles of urea-propyl modified silica with maximum coverage of functional groups provide better interactions with bilirubin molecules and, therefore, increase adsorption efficiency. When comparing the adsorption capacity of the obtained materials to adsorbents reported by other authors (Table 4), it can be concluded that the adsorbents prepared in this work have good adsorption capacity for bilirubin. The adsorption capacity of these adsorbents depends on the type of reactive ligands and experimental conditions (e.g. the conditions for bilirubin adsorption experiments). For instance, the adsorption capacity ofcyclodextrin-grafted polyethyleneimine is a bit higher than that of our functionalized silicas. But the organo-functionalized silicas have higher adsorption capacity compared to albumin modified silicas and poly-d-lysine immobilized chitosan particles. Also it should be indicated that there are some adsorbents based on nanocarbon exhibiting excellent adsorption properties for bilirubinin comparison with our materials. Thus, the difference of bilirubin adsorption is mostly due to the properties of each adsorbent: the morphological structure, specific surface area, total pore volume and average pore size, functional groups grafted onto surface.

4. Conclusions

Hybrid silicas functionalized with octyl, phenyl and urea-propyl groups were successfully prepared via sol–gel technique. The FTIR spectra of the obtained functionalized silicas confirmed the presence of functional groups. The morphological structure and surface properties of final products were tunable by varying the type of used organosilanes and the molar ratio of TEOS and co-precursors. The use of the functional organosilane co-precursors leads to generation of different morphology from plate-like structure to spherical nanoparticles. The functionalized silicas are characterized by the special interface properties for effective bilirubin binding and a good range of adsorption rate for

bilirubin. It was shown that bilirubin adsorption is affected by the type of functional-containing groups and their surface coverage. The urea-propyl functionalized silicas showed the largest binding ability for bilirubin from aqueous solution (pH 7.4) compared to octyl and phenyl functionalized silicas due to the presence of amine and carboxyl functional groups and uniform structure. The results show the good potential of these functionalized silicas as effective adsorbents for bilirubin removal.

Acknowledgments

We are grateful for support via a stipend of the President of the Russian Federation for study abroad in 2014–2015(http://www.president-mobility.ru/node/14) and the Ministry of Education and Science of the Russian Federation.

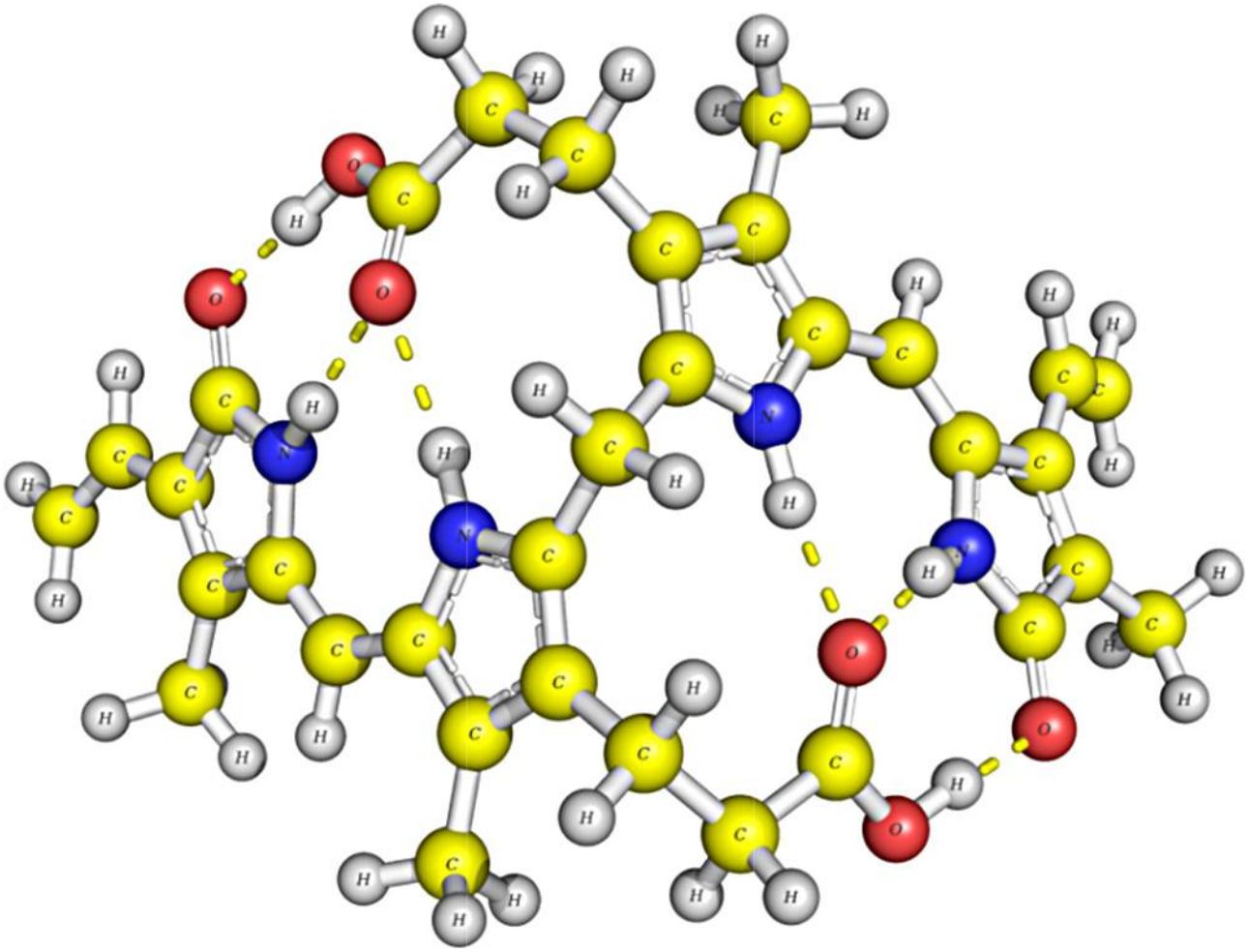

Fig. 1. Structure formula of bilirubin in “ridge-tile” 5Z, 15Z conformation stabilizedby six intramolecular hydrogen bonds.

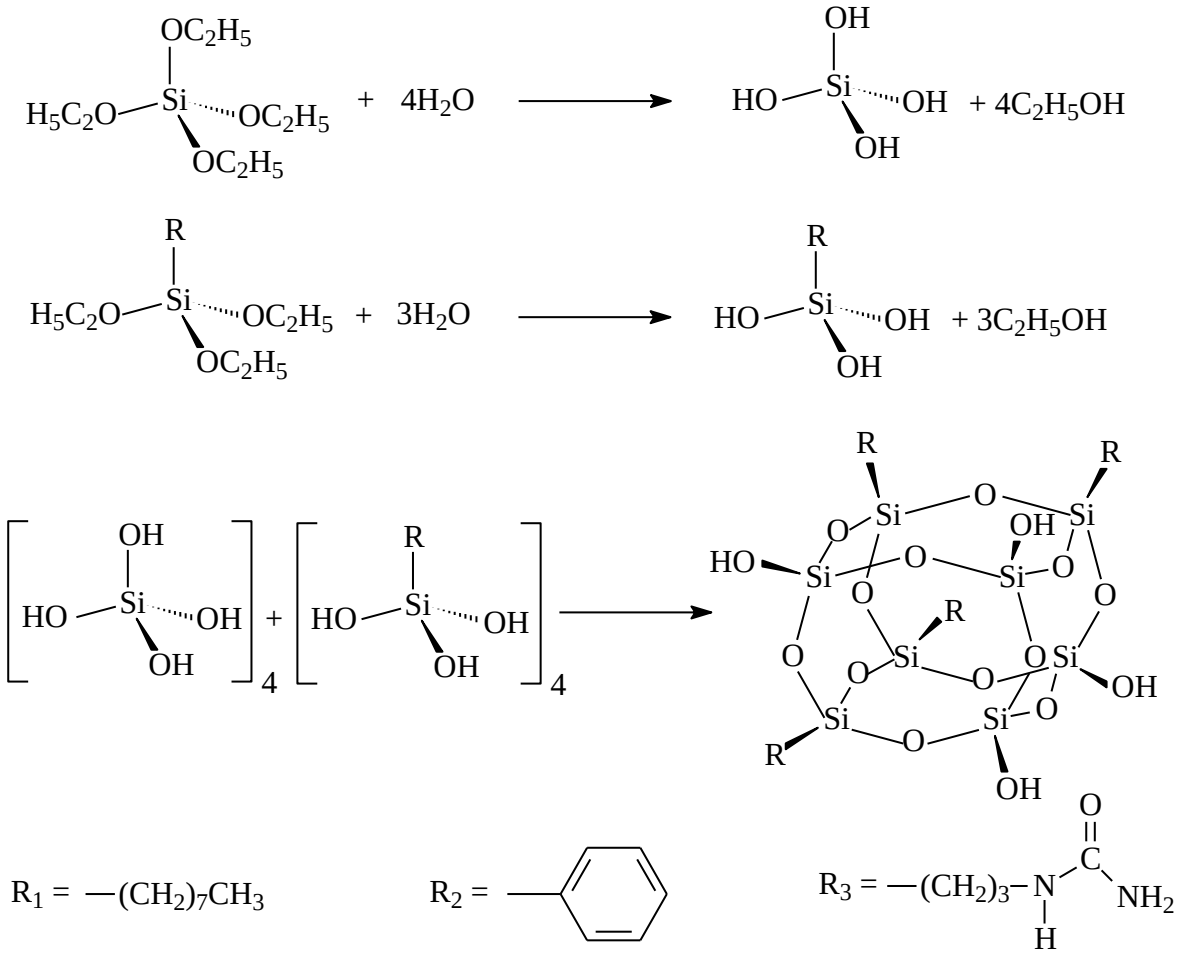

Fig. 2. Schematic representation of synthesis route of octyl, phenyl and urea-propyl functionalized silicas, respectively.

Table 1
Amount of silicon precursors used in the synthesis of the organo-functionalized silicas.

Samples	**TEOS/OTES (molar ratio)**	**OTES**	**TEOS**
SiNP	–	0	8.13
OctSiNP-1	4:1	1.82	6.48
OctSiNP-2	3:1	2.28	6.08
OctSiNP-3	2:1	3.05	5.41
Samples	TEOS/PhTES (molar ratio)	PhTES	TEOS
SiNP	–	0	8.13
PhSiNP-1	4:1	1.88	6.48
PhSiNP-2	3:1	2.34	6.08
PhSiNP-3	2:1	3.12	5.04
Samples	TEOS/TMSPU (molar ratio)	TMSPU	TEOS
SiNP	–	0	8.13
USiNP-1	4:1	1.74	6.48
USiNP-2	3:1	2.17	6.08
USiNP-3	2:1	2.89	5.04

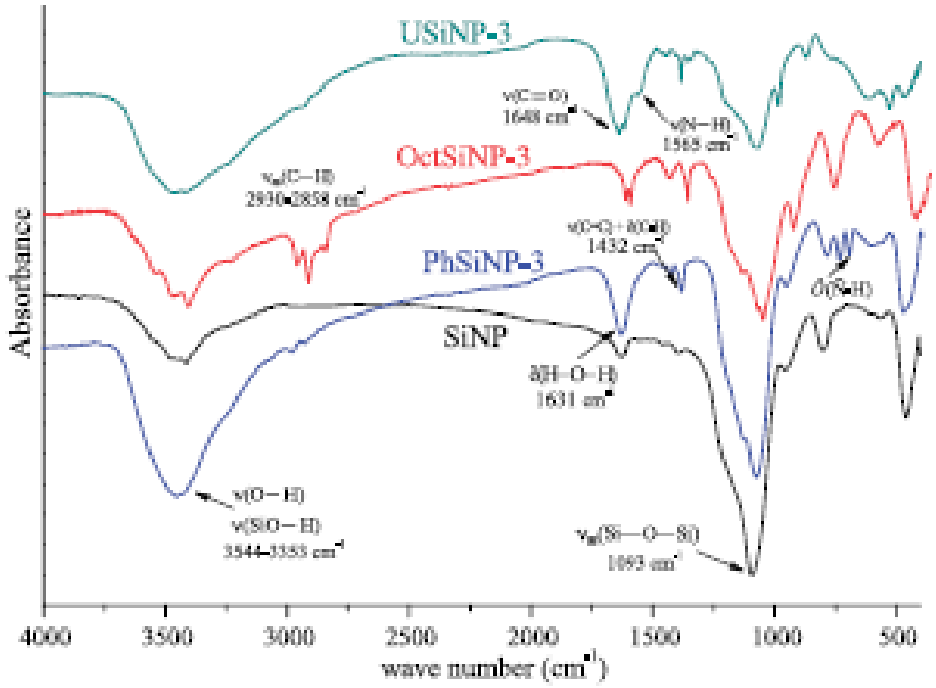

Fig. 3. FTIR spectra for pure and functionalized silicas with highest quantity of functional-containing groups. The FTIR patterns have been shifted for clarity.

Table 2
Characteristic vibration frequencies (cm^{-1}) in FTIR spectra of synthesized silica samples.

Octyl-functionalized silicas					
SiNP	OctSiNP-1	OctSiNP-2	OctSiNP-3	Type of vibrations	Structural unit
3452	3450	3461	3452	O—H and SiO—H	SiO–H···H_2O OH···H_2O
——	2929	2923	2925	ν_{as}(C—H)	$–CH_2$
	1633	1635	1633	δ(H—O—H)	H–O–H
1093	1081	1087	1081	ν_{as}(Si—O—Si)	≡Si–O–Si≡
800	794	794	788	ν_s(Si—O)	≡Si–O–Si≡
458	462	457	458	δ(Si—O—Si)	–O–Si–O–
Phenyl-functionalized silicas					
SiNP	PhSiNP-1	PhSiNP-2	PhSiNP-3	Type of vibrations	Structural unit
3452	3442	3440	3442	O—H and SiO—H	SiO–H···H_2O OH···H_2O
——	2979	2976	2975	ν_{as}(C—H)	$–CH_2$
——	1635	1635	1631	δ(H—O—H)	H–O–H
	1432	1431	1430	ν(C=C) + δ(C-H)	Si— Phenyl
1093	1079	1078	1081	ν_{as}(Si—O—Si)	≡Si–O–Si≡
800	792	789	790	ν_s(Si—O)	≡Si–O–Si≡
——	742	740	740	ω(C-H)	Si— Phenyl
——	700	701	700	*Ô*(Ñ-H)	Si— Phenyl
458	470	471	474	δ(Si—O—Si)	–O–Si–O–
Urea-propyl-functionalized silicas					
SiNP	USiNP-1	USiNP-2	USiNP-3	Type of vibrations	Structural unit
3452	3442	3446	3448	O—H and SiO—H	SiO–H···H_2O OH···H_2O
——	2941 weak	2942 weak	2935 weak	ν_{as}(C—H)	$–CH_2$
——	1648	1641	1641	ν(C=O)	C=O (Amide I)
——	1565	1560	1560	ν(N—H)	N—H (Amide II)
1093	1068	1076	1081	ν_{as}(Si—O—Si)	≡Si–O–Si≡
800	863 weak	865 weak	865	ν_s(Si—O)	≡Si–O–Si≡
458	451	453	457	δ(Si—O—Si)	–O–Si–O–

ν – stretching vibration; ν_s–symmetric stretching vibration; ν_{as} – unsymmetrical stretching vibration; δ –deformation vibration; *Φ*–out-of-plane ring deformation vibration; ω – in-phase out-of-plane wagging (the abbreviations of frequencies were used from [42]).

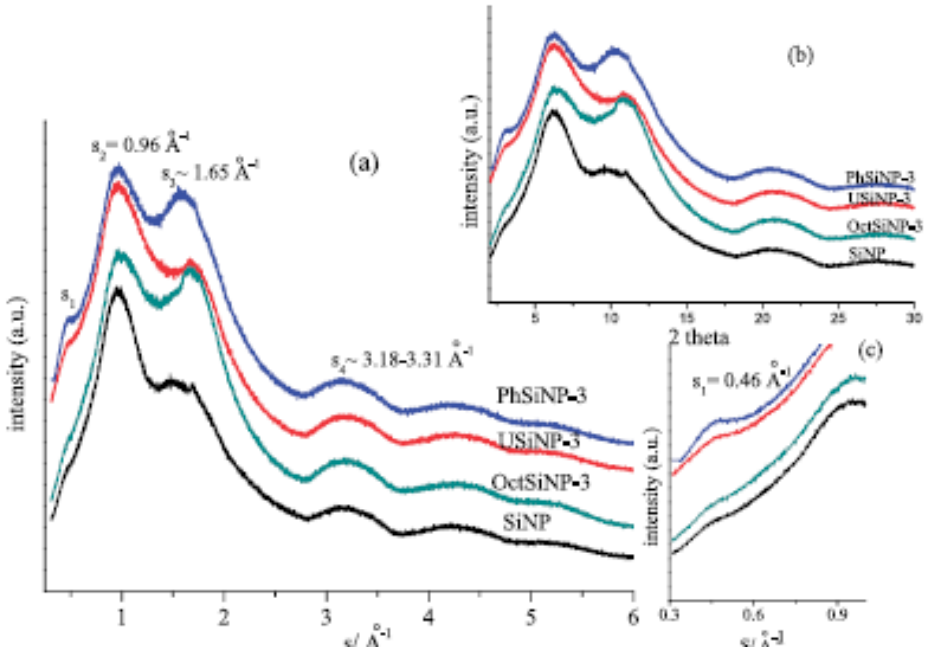

Fig. 4. XRD patterns of the pure amorphous and functionalized silicas in different coordinates on the X axis: $Å^{-1}$ (a, c); 2theta (b).

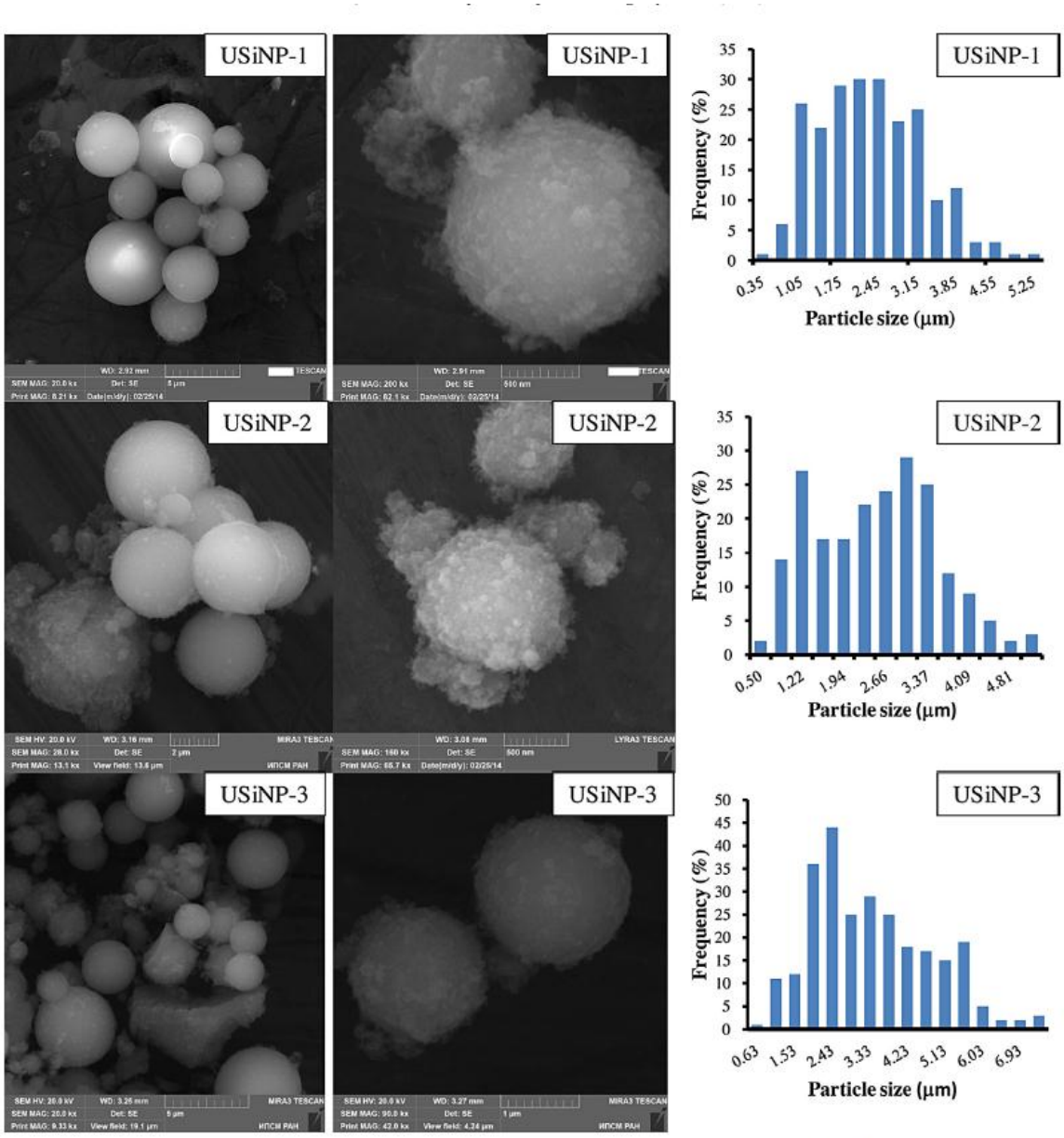

Fig. 5. SEM images of pure SiNP and urea-propyl functionalized silicas with their corresponding particle-size distribution histograms.

Fig. 5. SEM images of pure SiNP and urea-propyl functionalized silicas with their corresponding particle-size distribution histograms.

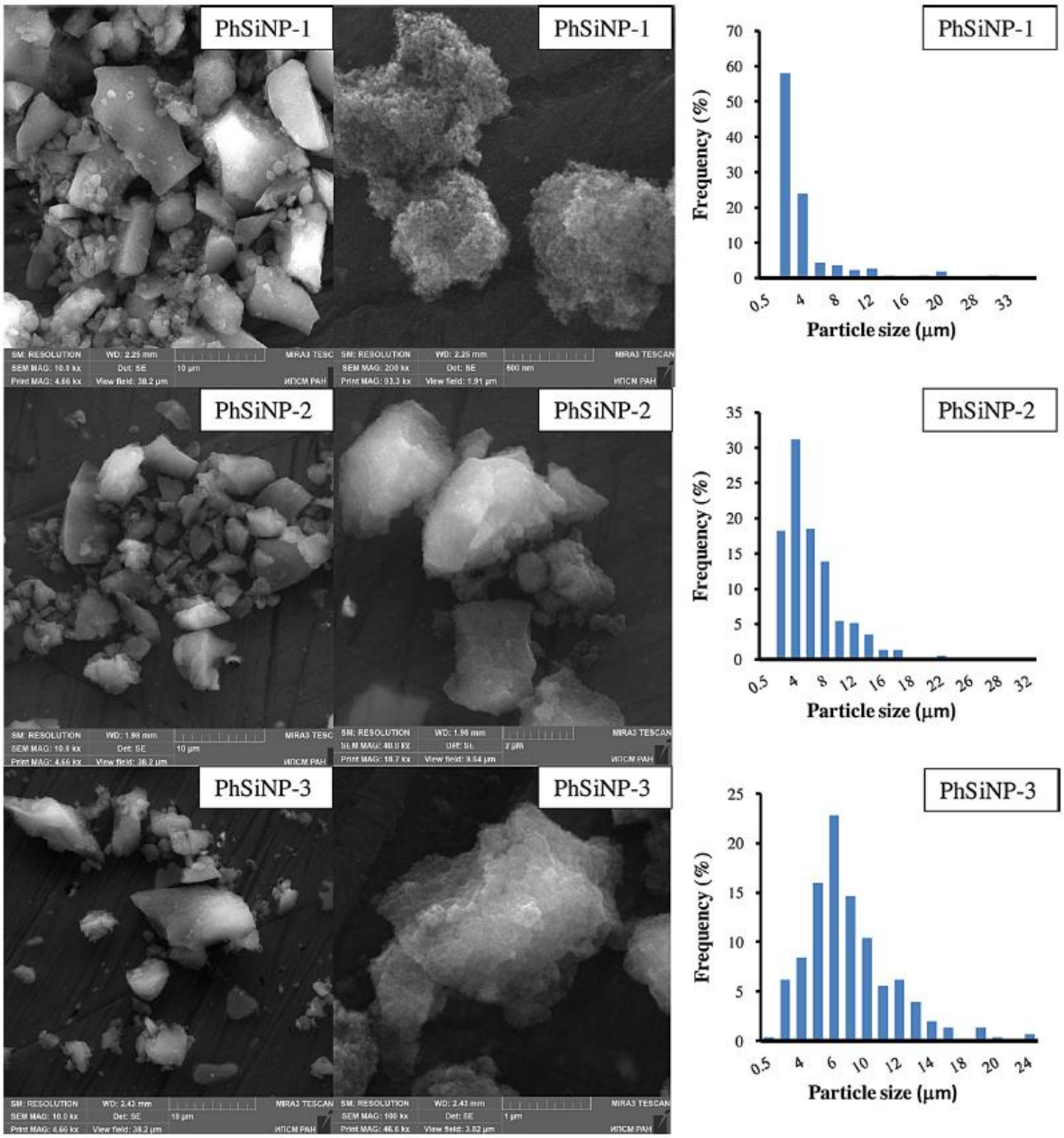

Fig. 6. SEM images of phenyl functionalized silicas with their corresponding particle-size distribution histograms.

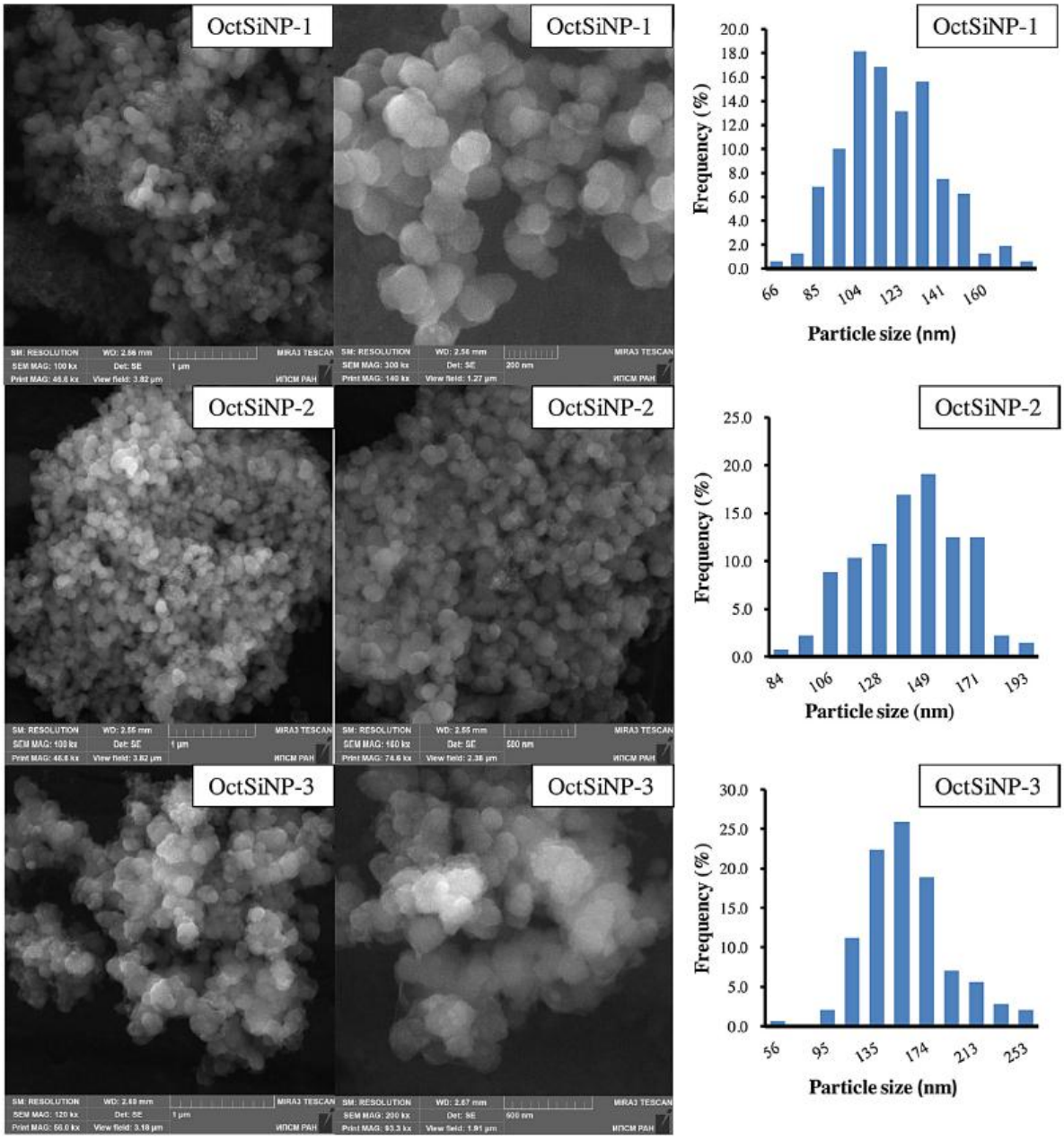

Fig. 7. SEM images of octyl-functionalized silicas with their corresponding particle-size distribution histograms.

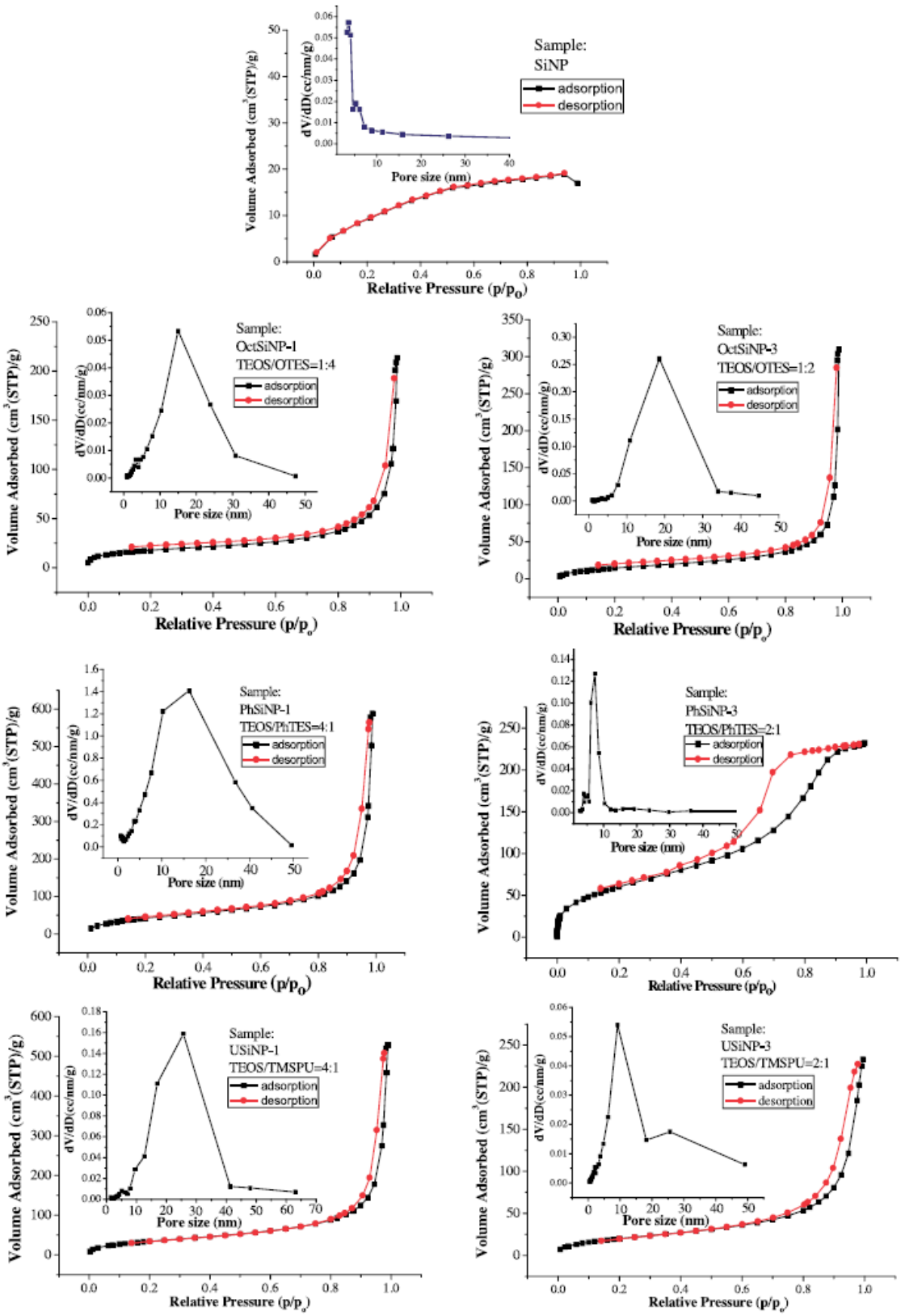

Fig. 8. The nitrogen adsorption isotherms and the corresponding pore-size distribution curves (inset).

Table 3
Physical parameters of the adsorbents measured by nitrogen adsorption–desorption isotherms.

Sample	BET surface area[a] (m^2/g)	Total pore volume[b] (cm^3/g)	Average pore diameter[c] (nm)
SiNP	40	0.015	2.6
Octyl functionalized silicas			
OctSiNP-1	91	0.32	16
OctSiNP-2	88	0.41	17
OctSiNP-3	84	0.48	19
Phenyl functionalized silicas			
PhSiNP-1	167	0.92	17
PhSiNP-2	232	0.51	10
PhSiNP-3	330	0.39	6.5
Urea-propyl functionalized silicas			
USiNP-1	141	0.42	25
USiNP-2	124	0.49	16
USiNP-3	105	0.54	11

[a] BET specific surface area measured in the 0.05–0.25 range of the relative pressures.
[b] Total pore volume was calculated at a relative pressure about 0.99.
[c] Average pore size was calculated from the BJH method.

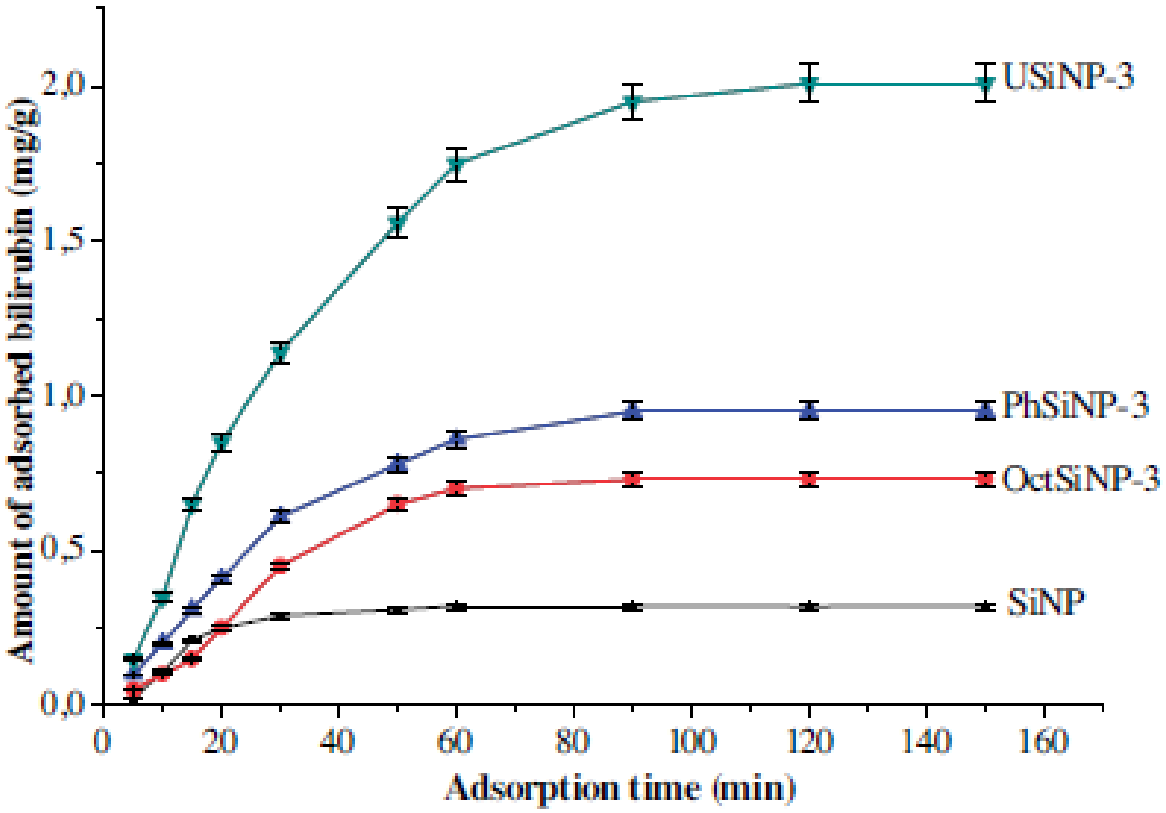

Fig. 9. Effect of time on the bilirubin adsorption for pure amorphous and function-alized silicas; V = 10 ml; m = 125 mg adsorbent, and T = 25◦C.

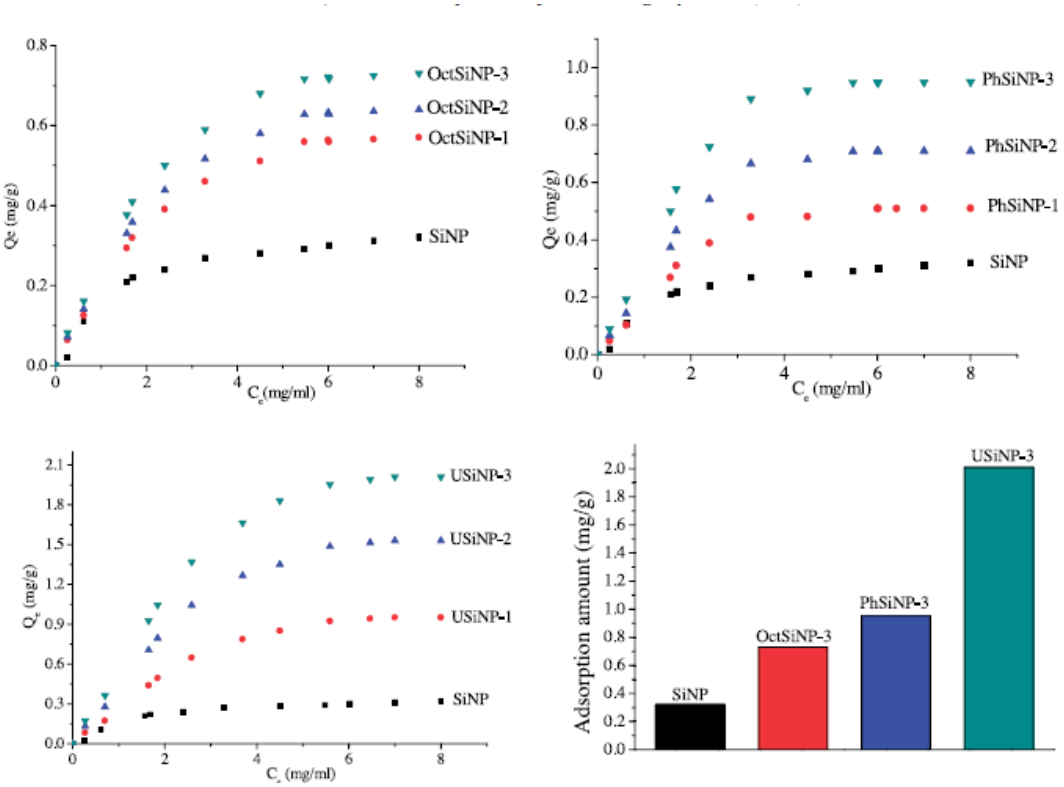

Fig. 10. Experimental adsorption isotherms of bilirubin for pure amorphous silica and organo-functionalized silicas; V = 10 ml; m = 125 mg adsorbent, and T = 25◦C.

Table 4
Adsorption capacity for bilirubin of modified adsorbents from the literature.

Material	Ligand (method of modification)	Adsorption capacity (mg/g)	Reference
polyethyleneimine	cyclodextrin	2.5	[34]
chitosan particles	poly-D-lysine	1.5	[54]
amino-modified silica particles	bovine serum albumin	1.17 – 1.65	[55]
silica particles	polymethacrylate guanidine	0.48 – 0.64	[38]
silica particles	polyacrylate guanidine	0.94 – 1.10	[38]
poly(HEMA-MAT)/MIP[a]	molecular recognition	3.41	[24]
cellulose acetate fiber	Cibaron Blue F3GA	4	[56]
Hollow mesoporous carbon spheres	High surface area, large pore size with narrow distribution	≈70	[26]
single-wall carbon nanohors	The size effect of nanopores	≈9.6	[37]
poly(MAA-EDGMA)/MIP[a]	molecular recognition	1.04	[57]
Octyl-functionalized silica	Octyltriethoxysilane	0.57 – 0.73	This study
Phenyl-functionalized silica	phenyltriethoxysilane	0.51 – 0.95	This study
Urea-propyl-functionalized silica	1-[3-(trimethoxysilyl)-propyl]urea	0.95 – 2.01	This study

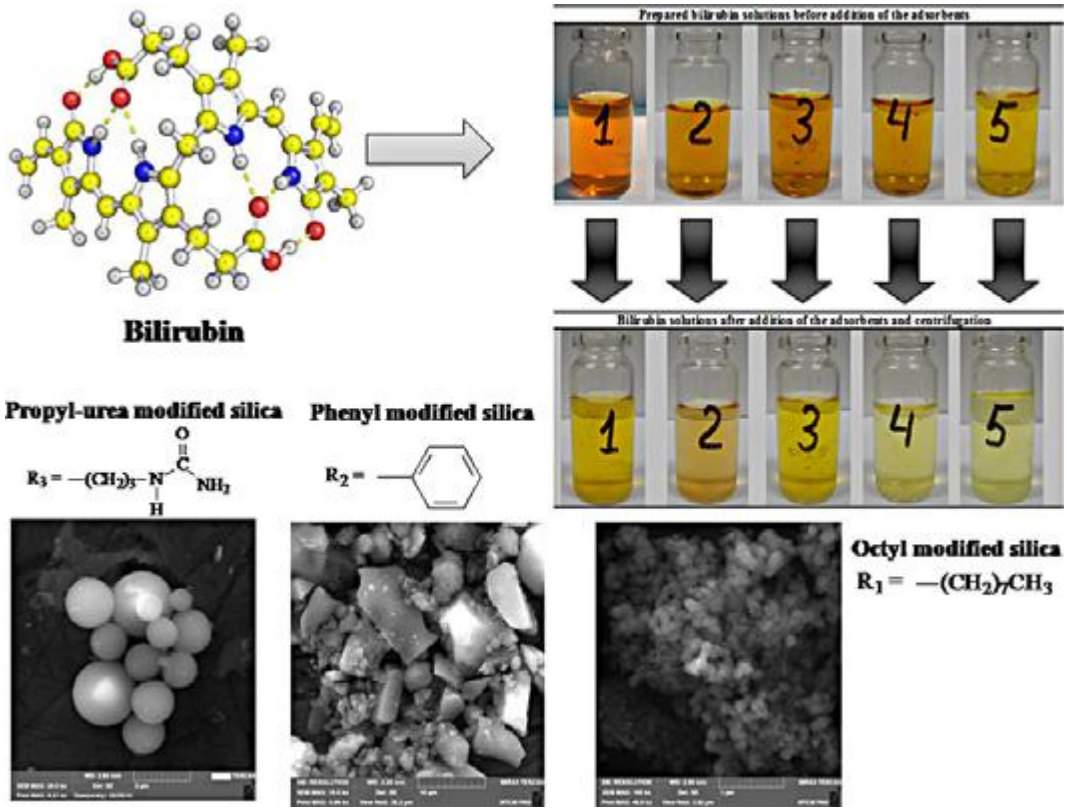

Graphical abstract

Highlights

- Organo-functionalized silicas were synthesized via sol–gel method.
- Functional groups have influence on morphological properties of the final products.
- The adsorption efficiency mostly depends on the type of surface functional groups.

References

[1] O.G. Silva, E.C.S. Filho, M.G. Fonseca, L.N.H. Arakaki, C. Airoldi, J. Colloid Interface Sci. 302 (2006) 485–491.

[2] Zhijian Wu, Xiang Hong, et al., J. Colloid Interface Sci. 304 (2006) 119–124.

[3] E.M. Bjork, F. Soderlind, M. Oden, J. Colloid Interface Sci. 413 (2014) 1–7.

[4] C.R. Miller, R. Vogel, P.P.T. Surawski, K.S. Jack, S.R. Corrie, M. Trau, Langmuir 21(2005) 9733.

[5] F. Xie, X. Lin, X. Wu, Z. Xie, Talanta 74 (2008) 836–843.

[6] D.P. Quintanilla, A. Sanches, I. Hierro, M. Fajardo, I. Sierra, J. Colloid InterfaceSci. 313 (2007) 551–562.

[7] J. Fan, C. Wu, Y. Wei, C. Peng, P. Peng, J. Hazard. Mater. 145 (2007) 323–330.

[8] Ieong Wong, Chih-Ming Ho, Microfluid Nanofluidics 7 (2009) 291–306.

[9] M.E. Valliant, F. Romer, et al., Acta Biomater. 9 (2013) 7662–7671.

[10] Wenjun Li, Minna Liu, C. Hongbiao, Jiao Xu, Gao Yong, Huaming Li, Polym. Adv. Technol. 25 (2014) 233–239.

[11] C. Sanchez, P. Belleville, M. Popall, L. Nicole, Chem. Soc. Rev. 40 (2011) 696–753.

[12] B.D. Louders, N.R. David, C.C. Mercedes, Chem. Soc. Rev. 36 (2007) 993–1017.

[13] Liangming Wei, Diwen Shi, et al., Nanoscale Res. Lett. 7 (2012) 334–342.

[14] A. Ishihara, T. Hashimoto, H. Nasu, Catalysis 2 (2012) 368–385.

[15] J.L. Vivero-Escoto, Michaël Carboni, C.W. Abney, K.E. deKrafft, W. Lin, Micropor. Mesopor. Mater. 180 (2013) 22–31.

[16] Sang-Eon Park, E.A. Prasetyanto, Top. Catal. 52 (2009) 91–100.

[17] A.S.O. Moscofian, M.T. Pires, A.P. Vieira, C. Airoldi, J. Porous Mater. 20 (2013) 1179–1188.

[18] F. Hoffman, M. Cornelius, J. Morell, M. Froba, Angew. Chem. Int. Ed. 45 (2006) 3216–3251.

[19] J. Kobler, K. Moller, T. Bein, ACS Nano 2 (2008) 791–799.

[20] G.E. Fryxell, S.V. Mattigod, Y. Lin, H. Wu, S. Fiskom, K. Parker, F. Zheng, W. Yantasee, T.S. Zemanian, R.S. Addleman, J. Liu, K. Kemner, S. Kelly, X. Feng, J. Mater. Chem. 17 (2007) 2863–2874.

[21] S.P. Le-Masurier, G. Gody, S. Perrier, A.M. Granville, Polym. Chem. 5 (2014) 2816–2823.

[22] P. Nabanita, A. Bhaumik, Adv. Colloids Interface Sci. 189–190 (2013) 21–41.
[23] P.A. Zunszain, J. Ghuman, A.F. McDonagh, S. Curry, J. Mol. Biol. 381 (2008) 394–406.
[24] G. Baydemir, MugeAndac, NilayBereli, et al., Ind. Eng. Chem. 46 (2007) 2843–2852.
[25] K.H. Lee, J. Wendon, M. Lee, Liver Transplant 8 (2002) 591–593.
[26] G. Limin, Z. Lingxia, Z. Jiamin, Z. Jian, et al., Chem. Commun. 40 (2009) 6071–6073.
[27] W.J. Holubek, R.S. Hoffman, D.S. Goldfarb, L.S. Nelson, Kidney Int. 74 (2008) 1327–1334.
[28] P.K. Tyagi, J.F. Winchester, D.A. Feinfeld, Kidney Int. 74 (2008) 1231–1233.
[29] N. Usharani, G.C. Jayakumar, J.R. Rao, et al., J. Microsc. 253 (2014) 109–118.
[30] J. Chen, G. Song, Yu. He, Q. Yan, Microchim. Acta 159 (2007) 79–85, http://dx.doi.org/10.1007/s00604-007-0736-9.
[31] A.V. Solomonov, E.V. Rumyantsev, S.P. Ivanov, B.A. Kochergin, E.V. Antina, Protein J. 32 (2013) 343–355.
[32] A.V. Solomonov, E.V. Rumyantsev, B.A. Kochergin, M.K. Serebryakova, P.V. Uckhov, E.V. Antina, FEBS J. 280 (1) (2013) 611.
[33] Ch. Zhiping, G. Baojia, Y. Xiaofeng, J. Chem. Sci. 121 (2009) 1061–1068.
[34] Z. Wang, Y. Cao, H. Wei, L. Jia, L. Xu, J. Xie, Colloids Surf.: B Biointerfaces 90(2012) 248–253.
[35] Shih-Kai Chou, Mei-Jywan Syu, Biomaterials 30 (2009) 1255–1262.
[36] B. Batra, S. Lata Sunny, J.S. Rana, C.S. Pundir, Biosens. Bioelectron. 44 (2013) 64.
[37] K. Yamazaki, K. Shinke, T. Ogino, Colloids Surf. B. Biointerfaces 112 (2013) 103–107.
[38] A.S. Timin, A.V. Solomonov, E.V. Rumyantsev, J. Polym. Res. 21 (2014) 400–409.
[39] A.S. Timin, E.V. Rumyantsev, J. Sol–Gel Sci. Technol. 67 (2013) 297–303.
[40] C.J. Brinker, G.W. Scherer, Sol–gel Science. The Physics and Chemistry of Sol–gelProcessing, Academic, New York, 1990, pp. 581–585.
[41] N.O. Gopal, K.V. Narasimhulu, J.L. Rao, Acta Part A 60 (2004) 2441.
[42] R. Al-Oweini, H. El-Rassy, J. Mol. Struct. 919 (2009) 140–145.
[43] N.B. Colthup, L.H. Daly, S.E. Wiberley (Eds.), Introduction to Infrared and RamanSpectroscopy, second ed., Academic Press, New York, 1975, p. 257.
[44] P. Huang, L. Zhiming, H. Hengyao, C. Daxiang, J. Nanomater. (2010),

http://dx.doi.org/10.1155/2010/641545.
[45] S. Boonurapeepinyo, N. Jearanaikoon, N. Sakkayawong, Int. Trans. J. Eng. 2(2011) 461–470.
[46] J.S. Beck, J.C. Vartuli, W.J. Rotz, M.E. Leonowicz, C.T. Kresge, K.T.C. Schmitt, T-W. Chu, D.H. Olson, E.W. Sheppard, S.B. McCullan, J.B. Higgins, J.L. Schlenker, J. Am. Chem. Soc. 114 (1992) 10834.
[47] L.A. Solovyov, O.V. Belousov, R.E. Dinnebier, A.N. Shmakovand, S.D. Kirik, J. Phys. Chem. B 109 (2005) 3233–3237.
[48] M. Ookawa, Y. Yogoro, T. Yamaguchi, K. Kawamura, Stud. Surf. Sci. Catal. doi: 10.1016/S0167-2991(01)81382-3.
[49] A.S. Timin, E.V. Rumyantsev, A.V. Solomonov, J. Non-Cryst. Solids 385 (2014) 81–88.
[50] F. Rouquerol, J. Rouquerol, K. Sing, Adsorption by Powders and Porous Solids, Academic Press, London, 1999, pp. 18–20.
[51] H. Ishida, S. Sato, A. Sannomiya, K. Tsuji, Transplant. Proc. 32 (2000) 2241.
[52] Z. Királyand, G.H. Findenegg, Langmuir 16 (2000) 8842–8849.
[53] Z. Boros, D. Weiser, M. Márkus, E. Abaháziová, A. Magyar, A. Tomin, B. Koczkac, P. Kovács, L. Poppe, Process Biochem. 48 (2013) 1039–1047.
[54] J. Crugeiras, A. Rios, E. Riveiros, J.P. Richard, J. Am. Chem. Soc. 133 (2011) 3173–3183.
[55] T. Chandy, C.P. Sharma, Artif. Organs 16 (1992) 568.
[56] Z. Ma, M. Kotaki, S. Ramakrishna, J. Membr. Sci. 265 (2005) 115–123.
[57] M.J. Syu, J.H. Deng, Y.M. Nian, T.C. Chiu, A.H. Wu, Biomaterials 26 (2005) 4684.